Locating air leaks in manned spacecraft using structure-borne noise

Stephen D. Holland,[a] D. E. Chimenti, Ron Roberts, and Michael Strei
Center for Nondestructive Evaluation, Iowa State Uninversity, Ames, Iowa 50011

(Received 27 July 2006; revised 4 March 2007; accepted 8 March 2007)

All manned spacecraft are vulnerable to leaks generated by micrometeorite or debris impacts. Methods for locating such leaks using leak-generated, structure-borne ultrasonic noise are discussed and demonstrated. Cross-correlations of ultrasonic noise waveforms from a leak into vacuum are used to find the location of the leak. Four methods for sensing and processing leak noise have been developed and tested and each of these can be used to reveal the leak location. The methods, based on phased-array, distributed sensor, and dual sensor approaches, utilize the propagation patterns of guided ultrasonic Lamb waves in the spacecraft skin structure to find the source or direction of the leak noise. It is shown that each method can be used to successfully locate the leak to within a few millimeters on a 0.6-m^2 aluminum plate. The relative merits of the four methods are discussed. [DOI: 10.1121/1.2722051]

PACS number(s): 43.40.Le, 43.40.Qi, 43.35.Zc, 43.35.Cg [WMC] Pages: 3484–3492

I. INTRODUCTION

Micrometeorites and space debris pose a constant danger to spacecraft in low-earth orbit. While the probability of a serious hit is quite low and large debris (>10 cm) can be avoided, small impacts routinely cause minor damage to the Space Shuttle and International Space Station.[1] The most dangerous debris, 0.5–100 mm in diameter, is too large to be stopped with certainty by shielding, but too small to be tracked and avoided.[2] An impact that penetrates the outer shielding and pressure vessel of a manned spacecraft will cause a leak that rapidly drains the limited air supply from the spacecraft. If the leak can be found rapidly and stopped, then the module can be salvaged. Otherwise, the crew will have no choice but to seal and abandon the module. In this paper, we demonstrate methods and algorithms for locating a single leak by monitoring leak-generated ultrasonic noise propagating within the skin of the spacecraft.

Our model for a leaking spacecraft is a 4.76-mm (3/16 in.) thick aluminum plate with a small hole and a vacuum behind the hole. This model is similar to the aluminum construction of the International Space Station. If a leak is present, turbulence in the leaking air will generate noise in the plate and in the air. Industrial off-the-shelf leak detectors for locating leaks in pressure vessels monitor airborne ultrasound near 40 kHz.[3] In the case of a leak into vacuum, the leak noise is generated by downstream turbulence at the exit and cannot travel up the Mach 1 free jet back into the spacecraft, where it might be detected. Instead, we exploit that portion of the leak noise that couples into the platelike skin of the spacecraft and is carried away from the leak site as guided ultrasonic Lamb waves. Our approach is to locate the leak by detecting and analyzing these guided waves. The theory and behavior of Lamb waves is well established, e.g., Ref. 4, and Lamb wave analysis is widely used as a tool for source location of acoustic emission signals.[5,6]

II. STATISTICAL SIGNAL ANALYSIS

The noise from the leak is inherently random. Moreover, it is so faint that it is often buried 20 dB or more under other noise sources. Therefore, instead of analyzing recorded noise waveforms directly, it makes sense to consider the statistics of the noise. In particular, we want to measure how sound waves detected by one sensor relate to sound waves detected by a second sensor, because this approach yields information about how the wave propagated to those sensors and hence the location of the noise source (the leak itself). The statistical tool that does this is cross-correlation,

$$\mathrm{XCORR}(x(t),y(t)) = \int_{-\infty}^{\infty} x(\tau)y(\tau - t)\, d\tau. \tag{1}$$

The cross-correlation at time t of two functions $x(t)$ and $y(t)$ is the inner product of x with y delayed by t, as given in Eq. (1). Cross-correlation is widely used industrially on leak-noise-generated guided mode waveforms to locate leaks in underground pipelines.[7–9] Cross-correlation transforms a pair of arbitrarily long noise waveforms captured simultaneously at different sensors into a composite waveform that represents the difference in propagation between the leak and each of the two sensors. Moreover, the cross-correlation is repeatable and predictable (ignoring variations from transducer coupling effects), and recording a full set of all possible cross-correlations (including autocorrelations) between sensors captures all possible useful information from those sensors about the leak. Cross-correlation also compresses extremely long measured noise waveforms into much shorter waveforms for processing and storage, and transforms very long measured noise waveforms with low signal-to-noise ratio (SNR) into shorter high-SNR correlations without loss of useful information.

[a]Address for correspondence: Iowa State University, ASC II, 1915 Scholl Road, Ames, IA 50011. Electronic mail: sdh4@iastate.edu

Let us consider a single frequency of leak-generated noise in an infinite plate. Assume the measurable amplitude of the noise in guided mode i is $|\tilde{A}_i|$ and its random phase is represented by the complex phase of $\tilde{A}_i$, which will generally be the same for the different modes. The noise in mode i at the location of the leak is

$$\tilde{A}_i \exp(j2\pi ft). \tag{2}$$

The waveform that would be measured at a distance d_1 from the leak is

$$\sum_i \tilde{A}_i \alpha_i \exp(j2\pi ft - jk_i d_1), \tag{3}$$

where k_i represents the frequency-dependent wave number of mode i and α_i represents combined the distance- and frequency-dependent attenuative effect of geometric diffraction, material absorbtion, and radiative loss (into the air). The cross-correlation between waveforms at distances d_1 and d_2 is

$$\sum_{i,l} |\tilde{A}_i||\tilde{A}_l| \alpha_i(d_1)\alpha_l(d_2) \exp(jk_i d_1 - jk_l d_2 + j2\pi ft), \tag{4}$$

or, ignoring the $i \neq l$ cross terms (thereby neglecting correlations between different modes),

$$\sum_i |\tilde{A}_i|^2 \alpha_i(d_1)\alpha_i(d_2) \exp[jk_i(d_1 - d_2) + j2\pi ft]. \tag{5}$$

The correlated noise is no longer random; the cross-correlation does not depend on the random phase of $\tilde{A}_i$, but only on its magnitude. From the point of view of waveform analysis the loss factors $\alpha_i(d_1)$ and $\alpha_i(d_2)$ are irrelevant because they vary slowly with frequency and hence affect only the broad spectrum of the waveform, but not its shape. When we ignore the loss terms and cross terms (or assume single mode propagation) the cross-correlation becomes a spatial function only of the difference in path lengths $d_1 - d_2$,

$$\sum_i |\tilde{A}_i|^2 \exp[jk_i(d_1 - d_2) + j2\pi ft]. \tag{6}$$

A propagating wave packet that arrives at both sensors simultaneously correlates at $t=0$, whereas a wave packet that arrives at one sensor 10 μs before the other correlates at either $t=10$ μs or $t=-10$ μs, depending upon which sensor the wave packet passed first. This dependence on the difference in distances can be counterintuitive. Because only the difference of distances is significant, sound need not come from the same location to correlate at the same time. A particular time in the cross-correlation maps through the modal wavespeed to a particular difference of distances. Geometrically, that difference of distances occurs along a hyperbola that has its foci at the sensor locations, so an observed arrival at that time could have come from any location on the hyperbola.

Successful source location is entirely dependent upon the leak noise being localized to a particular region of the plate by attenuation, edge absorption, and other losses. In a low-loss environment, reflected waves will interfere with direct waves, complicating the process of source location. In the extreme case of very low attenuation, resonance or a diffuse sound field can occur, and source location will become impossible because the cross-correlations will measure nothing but the resonance pattern and the Green's function between the sensors.[10] Since loss is in general a strong function of frequency, only a limited frequency range will contain useful information about the location of the leak. For our tests, we used frequencies between 200 and 600 kHz. Source location in small objects requires higher frequency measurement and analysis to assure sound field localization than source location in large objects, so lower frequencies may be more useful for actual spacecraft than in our small test configuration.

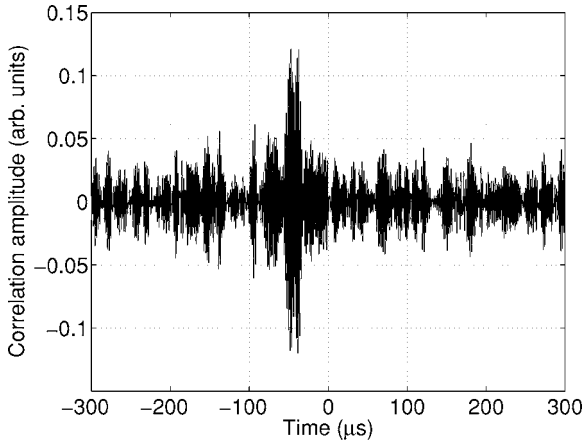

FIG. 1. A cross-correlation, filtered to eliminate low-frequency resonance.

Between 200 and 600 kHz and for our 4.76-mm plate thickness there are two detectible Lamb modes: the lowest order symmetric S_0 compressional mode and the lowest order asymmetric A_0 flexural mode. These two modes are both dispersive, in that their phase velocity depends on frequency. Their dispersion is reflected in the implicit frequency dependence of the wave number k in Eqs. (4)–(6). The dispersion relations $k_{A0}(f)$ and $k_{S0}(f)$ of the A_0 and S_0 Lamb modes can be readily calculated from the known material properties, thickness, and Lamb wave theory.[4] The two modes give rise to a total of four terms in Eq. (4), two single-mode terms plus two cross-terms. Therefore, the measured correlations will contain dispersed signals from the single-mode terms with interference from the cross-terms. Measured correlations tend to have distinct arrivals near $t=0$ or less distinct dispersed wavetrains at $t>0$ or $t<0$ depending on the magnitude and sign of the difference of distances $d_1 - d_2$. Figure 1 shows a (filtered) correlation waveform from measured data. A dispersed arrival can be seen near $t=-50$ μs. Assuming a wave speed of approximately 3 mm/μs, this translates to a difference of distances of approximately 150 mm.

Cross-correlation greatly reduces the amount of information that must be stored. Neglecting noise, the cross-correlation is only nonzero within a limited time window that comes from the total distances involved and the speed of propagation, so the cross-correlation is inherently compact, yet can represent data from arbitrarily long measured waveforms, since the integral in Eq. (1) goes out to infinity. Moreover, a full set of all possible autocorrelations (cross-

correlation of a waveform with itself) and cross-correlations between waveforms from a set of sensors is complete in the mathematical sense that it contains all possible useful information that could be extracted from the sensors. Therefore, storing and analyzing cross-correlations is an effective and efficient alternative to storing and analyzing the raw noise waveforms themselves.

We show by construction that noise waveforms equivalent to the originals can be calculated from the full set of auto- and cross-correlations, and therefore that there is no information loss from storing and processing only the correlations. Let $x(t)$, $y(t)$ be measured waveforms from a pair of sensors and $X(f)$, $Y(f)$ be their Fourier transforms. Since cross-correlation in the time domain is equivalent to multiplication by the complex conjugate in the frequency domain, the cross- and autocorrelations are $\mathrm{XCORR}(x,y)=X(f)Y^*(f)$, $\mathrm{XCORR}(x,x)=X(f)X^*(f)$, and $\mathrm{XCORR}(y,y)=Y(f)Y^*(f)$. These correlations can be measured to arbitrarily high signal-to-noise ratios by calculating them from sufficiently long recorded waveforms. First we reconstruct a frequency domain waveform $X_r(f)$ from the known amplitude spectrum $\sqrt{X(f)X^*(f)}$ and a single random function $\phi(f)$ giving random phase $e^{i\phi(f)}$. The inverse Fourier transform of $X_r(f)$ is the reconstructed noise waveform $x_r(t)$. The reconstructed noise waveform $Y_r(t)$ is the unique inverse Fourier transform of $Y_r(f)=[X(f)Y^*(f)/X_r(f)]$. Since the reconstruction is unique given $\phi(f)$, which is equivalent to (but different from) the random phase of the leak, the reconstructed waveforms are equivalent to the originals and there is no information loss in storing and processing only the correlations.

III. COUPLED TWO-DIMENSIONAL PHASED ARRAYS

Obviously a practical system for on-orbit spacecraft leak detection would need to have the fewest possible number of sensors because of measurement time and system complexity restraints. Nevertheless, to understand fully the problems and issues involved, we have collected an all-encompassing data set to represent what could be measured if time and complexity were irrelevant. Our data set contains all of the possible cross-correlations between elements of two two-dimensional phased arrays. Specialization of this data set was used to prototype the sparse methods to be described later.

A. Experimental measurements

An automated motion control system was used to position a pair of 1.5-mm-diam piezoelectric transducers used as sensors. Computer controlled stepping in 2-mm steps of each sensor over its own 32×32 mm^2 grid simulates two phased arrays on the 4.76-mm-thick aluminum plate. These phased arrays have been coupled by measuring correlations between signals from all possible pairs of locations in the two arrays. Figure 2 illustrates these arrays and the location of the leak. One-second long waveforms have been recorded at 5 megasamples per second (MSPS) for each pair of sensor locations. Cross-correlations are calculated from the recorded waveforms and stored. All possible cross-correlations between the 256 sensor positions in each array are recorded, leading to a total of 65 536 correlations arranged as a $(16\times16)\times(16\times16)$ phased array calculated from 655 billion samples.

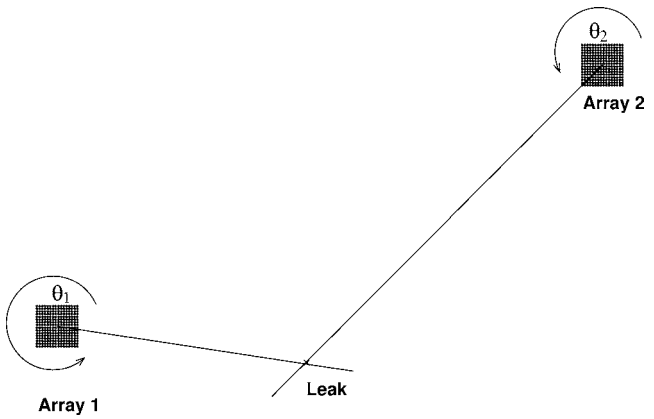

FIG. 2. Scale diagram of the four-dimensional phased array measurement. The leak is marked with an "x" and the lines indicate the measured vectors to the leak.

The processing of these data to reveal the leak location proceeds by straightforward Fourier phased-array analysis, followed by the application of *a priori* knowledge to reduce the dimensionality of the data from five dimensions to two. The raw correlation data $D(t,x_1,y_1,x_2,y_2)$ are discretely indexed along five dimensions: time, x_1, y_1, x_2, and y_2. A five-dimensional discrete Fourier transform converts the data to frequency-wavenumber space, $D(f,k_{x1},k_{y1},k_{x2},k_{y2})$. The transformed data set is then converted to polar coordinates, $D(f,|k_1|,\theta_1,|k_2|,\theta_2)$. One dimension can be eliminated from the data, along with the cross-terms of Eq. (4) by requiring the wave number magnitudes $|k_1|$ and $|k_2|$ to be equal at the two sensors and discarding all data not on the hyperplane $|k_1|=|k_2|$. The data can also be reduced in dimension by exploiting knowledge of the dispersion relations of the A_0 and S_0 modes, $k_{A0}(f)$ and $k_{S0}(f)$, to eliminate data not on the hyperplanes $|k|=k_{A0}(f)$ or $|k|=k_{S0}(f)$. The result of this reduction is a pair of three-dimensional data sets—one for A_0, one for S_0—each a function of f, θ_1, and θ_2. One more dimension can be eliminated by integrating the energy (square of the complex magnitude) of the data over frequency f, for example

$$D_{A0}(\theta_1,\theta_2)=\int_f \left|D(f,|k_1|,\theta_1,|k_2|,\theta_2)|_{|k_1|=|k_2|=k_{A0}(f)}\right|^2 df \quad (7)$$

for the A_0 mode. This leaves a pair (one for each mode) of two-dimensional functions of θ_1 and θ_2 that represent the modal energy from a common source incident on array 1 at angle θ_1 and on array 2 at angle θ_2.

B. Results

The A_0 and S_0 mode Eq. (7) energy integrals are plotted as grayscales in Fig. 3. The dark spots in Fig. 3 indicate the pairs of angles corresponding to coherent propagation past the two sensor arrays. The dark spots appear at exactly the same location for the A_0 and S_0 analyses, meaning that the

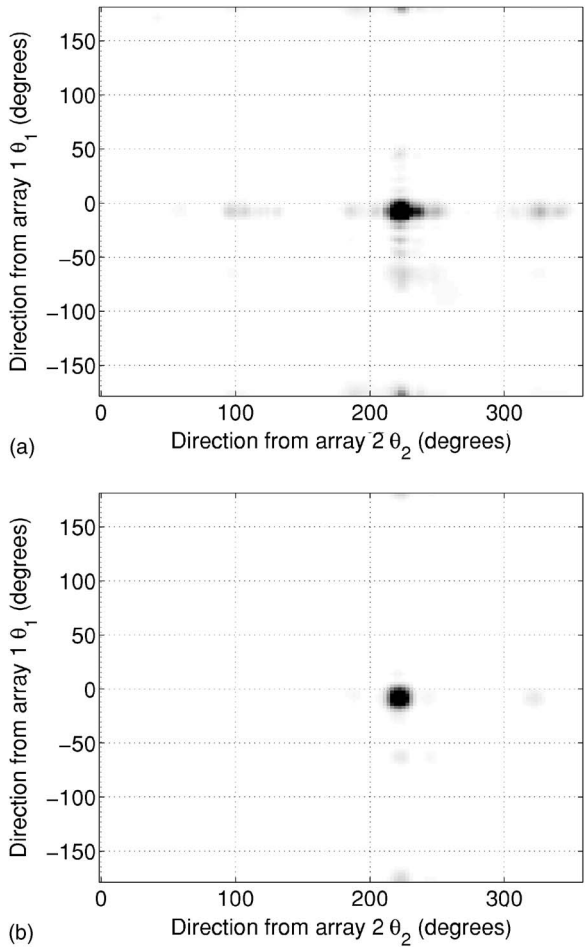

FIG. 3. Measured leak direction maps for (a) A_0 mode and (b) S_0 mode, both darkened by 100% to enhance visibility of interference.

location of the leak is independent of the mode selected for analysis. The measured propagation directions, from the location of the peaks (darkest points) in Fig. 3, are indicated as straight lines on Fig. 2, and their intersection provides an estimate of the location the source of the leak. In this case the estimated leak location is 1.8 mm from the actual location. To permit interference effects to be seen at all, the two images in Fig. 3 have been scaled in intensity by 100%. Interference is visible as faint spots on the figure away from the dark spots that indicate the primary directions. The interference comes from waves reflected by the boundary of our plate under test. Most of the interference spots are aligned vertically or horizontally with the primary spot, indicating a direct path from the leak to one sensor combined with a reflected path to the other sensor.

This measurement, while exhaustive in scope and impractical in terms of time and equipment, nonetheless demonstrates the capability to estimate the leak location accurately using random-signal guided waves. The coupled phased array method is particularly insensitive to interference and noise because only a tiny fraction of interference and noise are on the extracted hyperplanes; most interference and noise are distributed elsewhere in the five-dimensional space and are therefore suppressed. In order for interference to be visible at all in the measured data, Fig. 3 had to be scaled in intensity.

IV. TWO-DIMENSIONAL PHASED ARRAY

One strategy for reducing the quantity of data required is to reduce the coupled (x_1,y_1,x_2,y_2) array measurement described above to a pair of independent, two-dimensional array measurements: (x_1,y_1) and (x_2,y_2). For each array measurement, one sensor is fixed and the other is scanned across the 16×16 array. The number of correlations required for this measurement is $(16\times16)+(16\times16)=512$, a factor of 128 reduction in data from the 65 536 correlation full treatment. The three-dimensional (time, x, y) Fourier transform of the data from one sensor array gives a mapping of the directions of sound propagation in the vicinity of that array in terms of frequency and horizontal and vertical wave numbers. The three-dimensional transform given measured array waveforms $D(t,x,y)$ is

$$D(f,k_x,k_y)=\int_x\int_y\int_t D(t,x,y)\exp(-ik_xx-ik_yy-i2\pi ft)dt\,dy\,dx. \tag{8}$$

To display this as a two-dimensional image, we integrate the magnitude over our selected frequency range

$$D(k_x,k_y)=\int_{f_1}^{f_2}|D(f,k_x,k_y)|^2\,df \tag{9}$$

to obtain the distribution of energy in wave-number (k_x,k_y) space.

The bulk of the energy in wave-number space will be on a line emanating from the origin. The direction of this line is the direction to the leak, and the leak location can be therefore found by triangulation from two or more sensor assembly locations. The effect of decoupling the two arrays is that instead of correlating a specific mode crossing one array in one direction with the same mode crossing and the other array in the another direction, we can see only the angular energy distribution at each array. No longer is there any guarantee that the waves seen at one array match those at the other. In order to triangulate we have to assume the same waves are crossing both arrays, and, for example, in the unlikely event of multiple leaks, that assumption might be false.

A. Results

Because the required data for the two-dimensional phased array measurement are a subset of that required for the coupled measurement, instead of performing a separate experiment, we reprocess the data from the coupled experiment using only the required subset. We arbitrarily select one sensor position in sensor array 2 and extract the correlations with all possible sensor positions in sensor array 1 to obtain two-dimensional phased array data for sensor array 1 $D_1(t,x,y)$. Likewise, we select an arbitrary sensor position in array 1 and extract the correlations with array 2 to obtain phased array data for sensor array 2 $D_2(t,x,y)$. The data are processed using Eqs. (8) and (9). Figure 4 shows the pro-

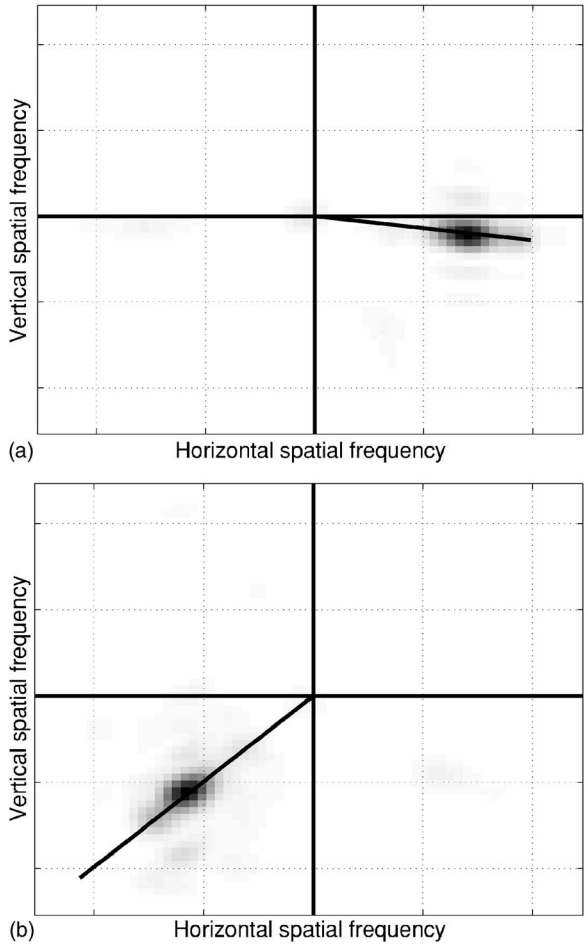

FIG. 4. Spatial frequency mapping of signal energy detected at (a) sensor array 1 and (b) sensor array 2. The black line indicates the measured direction to the source.

cessed two-dimensional phased array data from arrays 1 [Fig. 4(a)] and 2 [Fig. 4(b)]. The rays radiating from the origin in Fig. 4 indicate the measured θ_1 and θ_2 directions of −8 and 225 deg, respectively. Triangulation using these directions gives an estimated leak location 2.4 mm from the actual position of the leak on a 610×610-mm^2 plate compared with 1.8 mm when calculated from the coupled measurement. The leak location estimate of this method is nearly as accurate as the coupled measurement despite the massive reduction of data. Interference (darkened areas not on the rays) is visible in Fig. 4, even though Fig. 4 is not scaled in intensity. Interference and noise are higher than in the coupled case, in part because it has been constructed from far fewer data.

This method has the advantage that it requires far less information to find the leak location. It takes less acquisition time and less equipment than the full coupled measurement. Like the full algorithm, multimode propagation and dispersion will not create interference. Unlike the coupled method, this method treats each array independently. It finds the angular distribution of wave propagation independently under each array and triangulates from the apparently dominant direction. This two-dimensional phased array method provides a simple, robust method for locating leaks that requires far less data to be collected than the coupled phased array.

V. DISTRIBUTED DISCRETE SENSOR METHOD

While the two-dimensional phased array method requires far fewer correlations—and hence far less computation—than the four-dimensional method, it still requires two array sensors and hundreds of correlations. Using tiny subsets of the original coupled data set, we have developed an algorithm that locates the leak using only correlations between signals from a few isolated point sensors. This approach, which we have described briefly in Ref. 11, is more fully developed in Sec. V A. Our algorithm compares the measured correlations from a few arbitrarily distributed sensors with synthetic correlations calculated from all possible leak locations and identifies the closest match as the location of the leak.

A. Method and experiment

The method for locating the leak from the measured correlations has the following steps:

(1) Distribute a small number (four in our example) of sensors around a plate containing a leak, with known sensor locations $(x_1,y_1),\ldots,(x_4,y_4)$.
(2) Simultaneously record waveforms at all sensors $h_i(t)$, $i=1,\ldots,4$.
(3) Measure all (six) possible cross-correlations $R_{il}(t)=\int_\tau h_i(\tau)h_l(\tau-t)\,d\tau$ between noise waveforms from the four sensors, $R_{12}(t)$, $R_{13}(t)$, $R_{14}(t)$, $R_{23}(t)$, $R_{24}(t)$, $R_{34}(t)$.
(4) Calculate dispersion relations $k_{A0}(f)$ and $k_{S0}(f)$ for the two fundamental Lamb modes given the known thickness and material properties.
(5) Select one mode, A_0 or S_0.
(6) Select one measured correlation R.
(7) Select an arbitrary candidate leak location (x_x,y_c).
(8) Calculate a synthetic correlation R_s from Eq. (6), ignoring the loss factor α, assuming the leak is at the candidate leak location, assuming that only the selected mode is present, and assuming a flat frequency response over the selected frequency band.
(9) Calculate the inner product between the synthetic and measured correlations $\int_t R(t)R_s'(t)\,dt$.
(10) Repeat steps 7–9 for all candidate leak locations, generating a spatial mapping of the magnitude of the inner product, such as that shown in Fig. 5.
(11) Return to step 6 through step 10, multiplying the inner-product magnitudes for all the measured correlations to create a composite mapping, such as shown in Fig. 6(a) of leak intensity for the mode selected in step 5.
(12) Return to step 5, select another mode, and repeat all calculations through step 11, until all applicable modes have been accounted for. Sum the composite mappings to create an overall multi-mode map of leak intensity, as shown in Fig. 6(b).

The strongest peak in the overall multi-mode intensity map, such as Fig. 6(b), provides an estimate of the leak location.

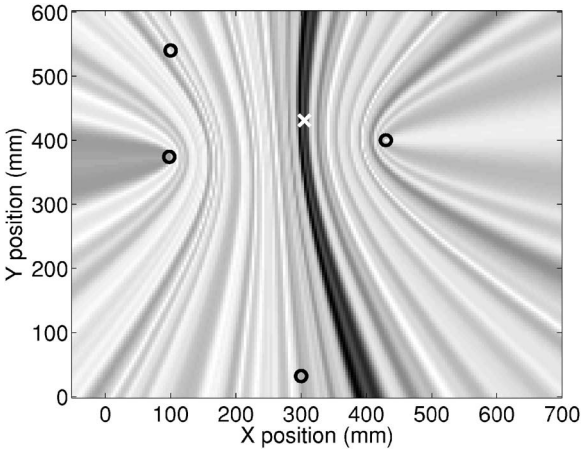

FIG. 5. Magnitude of the inner product of a measured correlation with S_0 synthetic waveforms as the assumed leak location varies spatially. The sensors are the "∘" symbols at the foci of the hyperbolas, and the actual leak location is marked with an "×".

B. Results

Because the algorithm processes the different modes independently, it is sensitive to both interference between the modes and interference from cross-terms. For example, a correlation signal from an A_0 wave mode but interpreted in the S_0 iteration could, when combined with interference in other correlations, generate a false peak in the S_0 map. To test the robustness of our procedure and to quantify the effect of this sort of interference, we have run a set of simulations with synthetic correlations assuming equal magnitudes of the A_0 and S_0 modes. These simulations are worst-case in the sense that equal A_0 and S_0 magnitudes give the highest possible relative amplitude of the cross-terms. We performed 32 simulation runs, each with a different, randomly selected, pattern of sensors. The average level of the cross-interference peak relative to the peak at the leak location is −5 dB. The largest interference peak observed is 4 dB stronger than the peak at the leak location in the overall map. Under worst-case circumstances with synthetic data, intermode interference can generate spurious peaks equal to, or larger than, the peak at the leak location. Nevertheless, in each of these cases the leak location is also predicted by means of a secondary peak. Since the interference is a function of the sensor layout pattern, careful placement can minimize interference effects. Adding sensors beyond the four probes assumed here will also tend to reduce interference. Experimental results from several sensor configurations with four probes are shown in Fig. 7. The actual location of the leak in a 610×610 mm^2 plate is found with a mean error of 10.4 mm in Figs. 7(a)–7(d). The arbitrarily distributed sensor method permits accurate, rapid leak location with a minimum of prepositioned equipment in an on-orbit spacecraft environment.

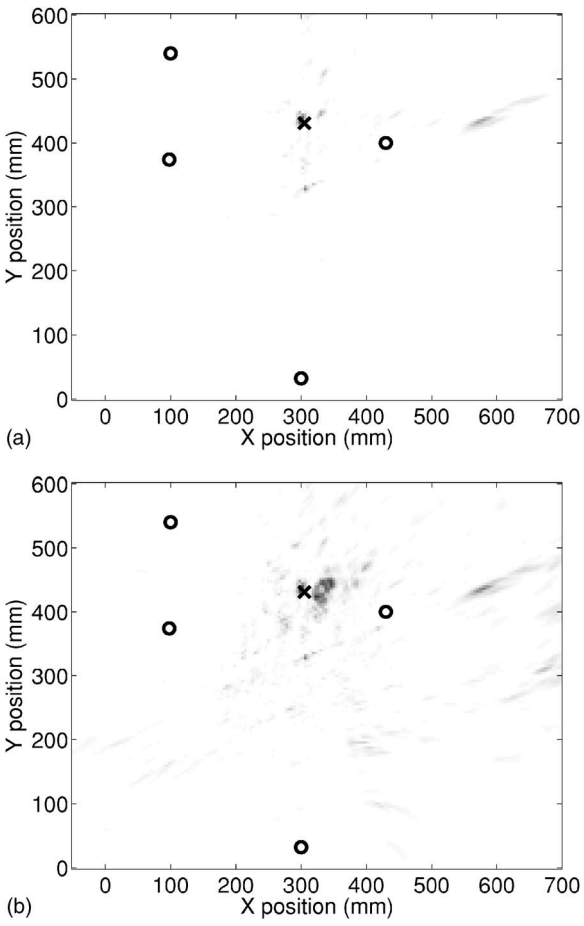

FIG. 6. (a) Product of S_0 inner product fields for all correlations (sensor pairs). (b) Sum of S_0 and A_0 products.

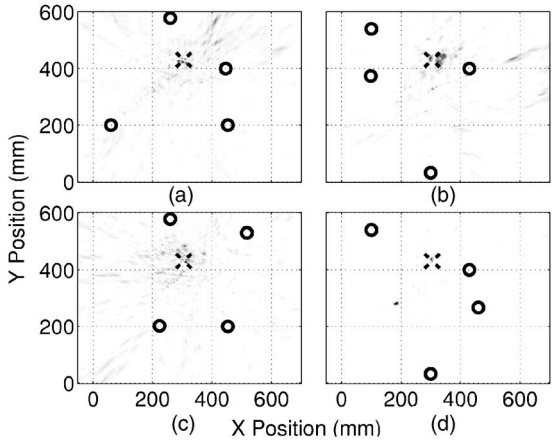

FIG. 7. Measured four-sensor source location solutions for four different sensor configurations.

VI. TWO-SENSOR METHOD

Another sparse-detector method uses two rotatable sensors. This method is appropriate for cases where a portion of the inner surface of the spacecraft pressure vessel is directly accessible to astronauts, and is suitable for smaller leaks for which the inherent delay involved in a manual measurement will not be a hazard. As we have previously discussed in a preliminary report,[12] by rotating a pair of sensors around a central point, correlation data can be collected that can be processed by a differential phase analysis or a circular synthetic aperture analysis to determine the direction of sound wave propagation. As in the phased array methods, triangulation from two or more measurement positions will locate the leak.

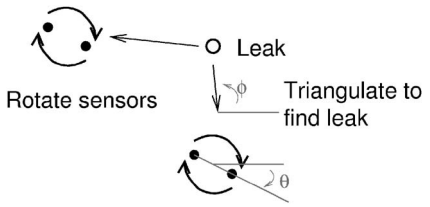

FIG. 8. Diagram showing rotation of sensors and triangulation to find leak.

A. Method and experiment

At each of two or more locations, a pair of rotatable sensors is held at a fixed separation and correlations are recorded as the sensor assembly is rotated in 15-deg increments, as illustrated in Fig. 8. The direction to the leak is found by examining the phase of the Fourier transforms of these correlations as a function of angle. Assuming a single mode incident at angle ϕ on the sensor pair rotated to angle θ, the correlation of the signals from the two sensors (separation d) will be

$$|\tilde{A}|^2 \exp\left[j2\pi ft - jkd\cos(\theta-\phi)\right]. \tag{10}$$

The phase of the Fourier transform of the correlation is $-jkd\cos(\theta-\phi)$. The phase varies sinusoidally as the sensor assembly is rotated, with the zeroes of the sinusoid occuring when the line connecting the sensors is parallel to the propagating wavefronts. The extrema of the phase occur when that line is perpendicular to the propagating wavefronts. Figure 9 shows the magnitude of the inner product

$$P(f) = \sum_{\theta} \text{angle}^{(\text{unwrapped})}(D(f,\theta))e^{j\theta} \tag{11}$$

of the unwrapped phase of a set of measured correlations with a 360 deg complex sinusoid, where $D(f,\theta)$ is the temporal Fourier transform of the measured correlation at sensor assembly angle θ. The dashed and dotted lines in Fig. 9 show expected magnitudes of the inner product assuming propagation in the flexural (A_0) and compressional (S_0) modes, respectively. In order for the phase variation to be a meaningful measure of leak direction, there must be a single dominant mode propagating at each frequency, because multiple modes propagating together will cause phase interference. Figure 9 demonstrates which mode is usable in which frequency range. In this case, the data indicate that the compressional (S_0) mode dominates from 450 to 540 kHz as marked on the plot, that the fiexural (A_0) mode dominates from 280 to 375 kHz, and that other ranges, showing large rapid fluctuations, exhibit interference between the modes. Once a frequency range has been selected the angle to the leak can be estimated by calculating the median phase over the selected frequency range of $P(f)$ from Eq. (11),

$$\underset{f}{\text{median}}[\text{angle}(P(f))]. \tag{12}$$

Angles calculated with Eq. (12) are then triangulated from two or more measurement locations to precisely locate the leak.

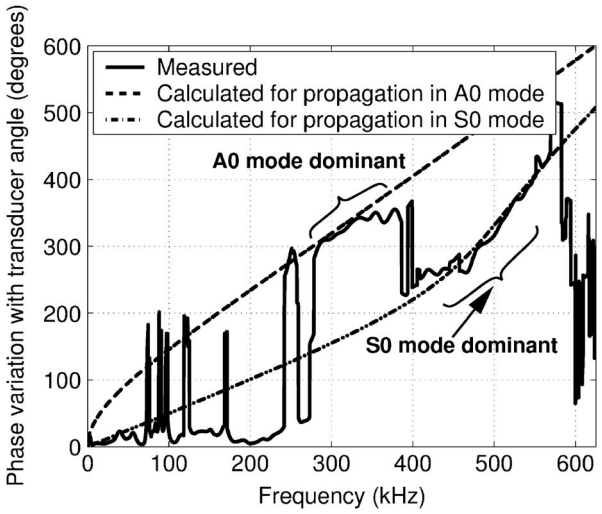

FIG. 9. Variation of phase with sensor angle, measured and calculated for A_0 and S_0 modes.

Another way to analyze these data is as a circular synthetic aperture.[13] Unlike the rectangular synthetic aperture (phased array) analysis described earlier, the basis functions of the circular synthetic aperture are nonorthogonal. Therefore, calculating the angular spectrum from the circular array data is an ill-posed inversion problem. To accomplish the inversion we use below a modified Lanczos matrix pseudoinverse, similar to that discussed by Jackson.[14]

If a sound wave is incident upon the circular synthetic aperture location at angle ϕ, and the sensor assembly, with element separation d, is rotated to direction θ, then the expected correlation [from the simplified correlation of Eq. (6)] would be

$$\sum_i |\tilde{A}_i|^2 \exp\left[j2\pi ft - jk_i d\cos(\theta-\phi)\right], \tag{13}$$

where the sum is over the mode index i. In the synthetic aperture analysis we assume incident waves in every possible direction and then solve for the amplitudes of those waves given the measured correlations. Let $\tilde{A}_{mi}$ be the amplitude and phase of the incident wave propagating in the direction ϕ_m in mode i. The measured cross-correlations with the sensor assembly at angle θ_l would be

$$\text{XCORR}_l = \sum_m \sum_i |\tilde{A}_{mi}|^2 \exp\left[j2\pi ft - jk_i d\cos(\theta_l-\phi_m)\right]. \tag{14}$$

To solve the synthetic aperture problem, we must solve for the angular and modal amplitude spectra $|\tilde{A}_{mi}|$ given the measured cross-correlations. Equation (14) can be represented as a matrix multiply. Let $D_{lmi} \equiv \exp\left[-jk_i d\cos(\theta_l-\phi_m)\right]$. At each frequency f we can construct a matrix $E_{lq} \equiv [D_{lmA_0} D_{lmS_0}]$ and a vector $C_q \equiv \begin{bmatrix} |\tilde{A}_{mA_0}|^2 \\ |\tilde{A}_{mS_0}|^2 \end{bmatrix}$ such that Eq. (14) reduced to the matrix equation

$$\text{XCORR}_l = \sum_q E_{lq} C_q \exp(j2\pi ft). \tag{15}$$

Equation (15) represents the prediction of correlations from a known angular and modal spectrum C_q as a matrix multipli-

cation. Inversion of this equation allows estimation of the angular distribution of incident waves from the measured data. In a linear synthetic aperture problem, E_{lq} is a spatial Fourier transform and is easily inverted. In the current case of a circular synthetic aperture, depending on the number of chosen values for ϕ_m and θ_l, this matrix is ill conditioned and may not be square. To construct the pseudoinverse E_{lq}^{inv}, we first calculate the singular value decomposition of E, $E = USV^t$, where U and V are unitary and S is diagonal, with its elements S_{ii} the singular values. Let the largest singular value be $S_{\max}$. The pseudoinverse is $E^{\text{inv}} = VS^{\text{inv}}U^t$, where S^{inv} is diagonal and constructed from the elements of S,

$$S_{ii}^{\text{inv}} = \frac{1}{S_{ii}} e^{-0.2(S_{\max}/S_{ii}-1)} \quad \text{(no sum)}. \tag{16}$$

Since E is ill conditioned, it likely has very small singular values. When inverted, these small singular values become very large and potentially scale any error or noise in the measured correlations. The exponential factor in Eq. (16) limits the noise gain of the inversion process by scaling down the inverses of the smallest singular values, following the concept of singular value truncation discussed in Ref. 14. The arbitrary factor of 0.2 selects the rate of scaling and corresponds to the reduction of the inverse of a singular value with half the magnitude of the largest singular value.

The estimated angular and modal distribution can be calculated from E_{ql}^{inv} according to

$$\begin{bmatrix} |\hat{\tilde{A}}_{mA_0}|^2 \\ |\hat{\tilde{A}}_{mS_0}|^2 \end{bmatrix} \equiv \hat{C}_q = \sum_l E_{ql}^{\text{inv}} \text{XCORR}_l e^{-j2\pi ft}. \tag{17}$$

Equation (17) gives the synthetic aperture calculation for estimating the incident angular and modal distribution $|\hat{\tilde{A}}_{mi}|^2$ from a single frequency component (at frequency f) of a set of measured correlations XCORR_l. By iterating this calculation over our frequency range, we obtain the estimated angular distribution as a function of frequency and mode. Integrating this distribution over frequency,

$$\int_{f_1}^{f^2} |\hat{\tilde{A}}_{mi}|^2 \, df, \tag{18}$$

will yield a peak in the integral in the dominant direction. This peak gives an estimate of the direction to the source. Figure 10 shows an example angular and modal distribution from experimental data, calculated using the circular synthetic aperture method.

Figure 11 shows an example of two-sensor leak location by triangulation from three measurement positions using both analysis methods. The solid discs indicate the measurement positions, and rays emanating from them indicate the estimated directions to the leak as determined by the two algorithms. The leak itself is located at the origin, and the estimated location is marked with an open circle is at coordinates (17 mm, 3 mm). The source location error in this case was 2.0 mm for the phase comparison method and 2.3 mm for the circular synthetic aperture method. As before, this source location was accomplished using a 610 mm^2 4.76-mm-thick aluminum plate with a l-mm-diam leak. The two-sensor method is a viable method for locating leaks. It has the disadvantages of requiring manual operation and high sensitivity to cross-mode interference, yet it requires a minimum of equipment. Unlike the other methods the equipment would not need to be manufactured as part of the spacecraft.

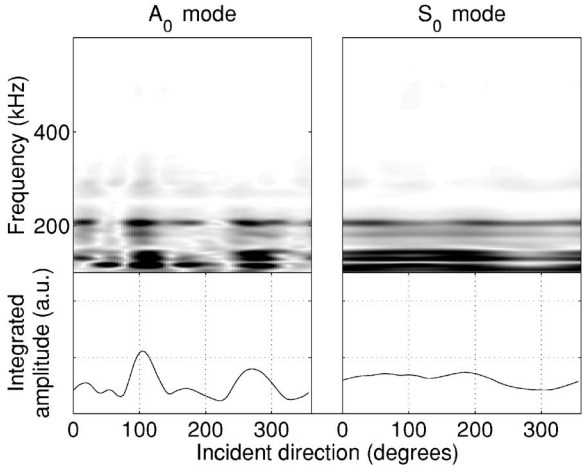

FIG. 10. Example measured angular and modal distribution from circular synthetic aperture method.

VII. CONCLUSIONS

Each of these methods developed and demonstrated here can successfully and repeatably locate air leaks into vacuum using structure-borne noise. Of the four methods, only the first—the four-dimensional phased array—is wholly impractical because of the extreme amount of data that must be collected. Each of the other methods is a viable alternative depending on the circumstances involved. We anticipate that the two-dimensional phased array could be made practical by using a miniature array transducer with high speed correlator

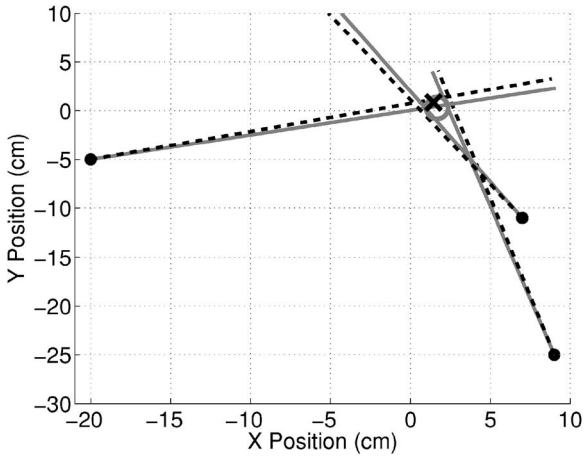

FIG. 11. Example leak location with two movable sensors. Each location of the sensor pair is marked with a disc. The measured directions to the leak with the phase comparison algorithm are shown as solid gray lines. Measured directions with the circular synthetic aperture method are shown as dashed black lines. The least-squares measured location of the leak is marked with a circle (phase comparison) and "×" (synthetic aperture). For comparison, the actual leak location was the origin (0,0).

electronics, and we are actively developing a miniature 8 $\times$8 array for this purpose. With a scattering of two-dimensional arrays on the inside of a spacecraft module, this method would instantly identify the location of the leak while rejecting possible interference. The distributed discrete sensor method would provide the same result, but with greater vulnerability to interference and false peaks, yet with substantially smaller hardware and computation requirements. The two-sensor method would be appropriate for the more spartan spacecraft environment in which the outer pressure walls are accessible from the inside and for which the weight of permanently embedded monitoring system would be prohibitive.

We have discussed the problem of locating air leaks in manned spacecraft. We have shown how cross-correlation can be used to transform the leak noise into a quantity that can be usefully measured, and described and demonstrated a series of algorithms for collecting and analyzing these cross-correlations to determine the location of a leak. Each of the methods works repeatably, and each is suitable for different circumstances. By applying these methods to manned spacecraft, the risk of micrometeorites and space debris to the mission and to the crew can be dramatically reduced.

ACKNOWLEDGMENT

This material is based on work supported by NASA under Award No. NAG-1-029098.

[1]L. Foster, J. Frisbee, M. Wortham, and L. Howorth, "International Space Station Debris Avoidance Operations," The Orbital Debris Quarterly News **6**(2), 4–5 (2001) http://www.orbitaldebris.jsc.nasa.gov/newsletter/newsletter.html(verified 4 March 2007).

[2]Committee on Space Shuttle Meteoroid/Debris Risk Management, NRC, *Protecting the Space Shuttle from Meteoroids and Orbital Debris* (National Academies Press, Washington, DC, 1997).

[3]G. Studor, "Ultrasonic detectors in space," http://www.ctrlsys.com/library/articles/index.php(verified 4 March 2007).

[4]A. H. Nayfeh, *Wave Propagation in Layered Anisotropic Media* (Elsevier, Amsterdam, 1995).

[5]W. H. Sachse and S. Sancar, "Acoustic emission source location on plate-like structures using a small array of transducers," US Patent #4,592,034 (1986).

[6]M. R. Gorman, "Plate wave acoustic emission," J. Acoust. Soc. Am. **90**(1), 358–364 (1991).

[7]D. S. Kupperman, "Detector relies on sound to locate underground pipe leaks," Power **134**(2), 61–62 (1990).

[8]J. Golby and T. Woodward, "Find that leak," IEE Rev. **45**(5), 219–221 (1999).

[9]L. E. Rewerts, R. A. Roberts, and M. A. Clark, "Dispersion Compensation in Acoustic Emission Pipeline Leak Location," in *Review of Progress in QNDE*, edited by D. O. Thompson and D. E. Chimenti (AIP, New York, 1997), Vol. **16**, pp. 427–434.

[10]R. L. Weaver and O. I. Lobkis, "Ultrasonics without a Source: Thermal Fluctuation Correlations at MHz Frequencies," Phys. Rev. Lett. **87**, 134301 (2001).

[11]S. D. Holland, R. Roberts, D. E. Chimenti, and M. Strei, "Leak detection in spacecraft using structure-borne noise with distributed sensors," Appl. Phys. Lett. **86**, 174105 (2005).

[12]S. D. Holland, R. Roberts, D. E. Chimenti, and M. Strei, "Two sensor ultrasonic spacecraft leak detection using structure-borne noise," ARLO **6**(2), 63–105 (2005).

[13]N. Yen, "A circular passive synthetic array: An inverse problem approach," IEEE J. Ocean. Eng. **17**(1), 40–47 (1992).

[14]D. D. Jackson, "Interpretation of inaccurate, insufficient and inconsistent data," Geophys. J. R. Astron. Soc. **28**, 97–109 (1972).